PARAMETER OPTIMISATION OF INDIVIDUAL CELLS THROUGH VOLTAGE DEPENDENT ELECTROLUMINESCENCE OF AN EXPERIMENTAL SILICON MODULE

Ross M Dix-Peek[1], Isaac Kwembur[2], E Ernest van Dyk[3], Frederik J Vorster[4], and Christiaan J Pretorius[5]

[1] Nelson Mandela University, University Way, Port Elizabeth, South Africa, Phone: +27 41 504 2233, E-Mail: s212286552@mandela.ac.za

[2] Nelson Mandela University, E-Mail: s215379446@mandela.ac.za

[3] Nelson Mandela University, E-Mail: Ernest.vanDyk@mandela.ac.za

[4] Nelson Mandela University, E-Mail: Frederik.Vorster@mandela.ac.za

[5] Nelson Mandela University, E-Mail: Christiaan.Pretorius@mandela.ac.za

Abstract

This paper outlines a method which can be used to non-destructively characterise individual Photovoltaic (PV) cell Current-Voltage (IV) data for cells encapsulated within a module.

In this study a Genetic Algorithm (GA) for the Parameter Optimisation (PA) is used to determine the electrical parameters of individual PV cells within a module using voltage dependent Electroluminescence (EL) data in conjunction with dark (current voltage) IV data of the module. This is the first step in studying the deconvolution of the IV curve of a module.

Keywords: Genetic Algorithm; Parameter Optimisation; IV curve; Electroluminescence

1. Introduction

This paper outlines the basic theoretical background and experimental procedure required to isolate the individual solar cell electrical characteristics from the electrical and electroluminescence data from a complete module.

In this study, the electrical parameters are obtained by the application of a GA for PO on the measured module current and the calculated cell voltage.

Such a method can be used by researchers to study cell degradation and mismatch within modules. This technique can further be implemented in industry to quantify the Electroluminescence (EL) data acquired from modules and used to potentially identify the source of power degradation of an operational PV power plant.

2. Theoretical Framework

2.1. Electrical characteristics

The IV relationship of a solar cell can be modelled using either the one- or two-diode model [1]. In the case of this study, the two-diode model was applied to the data. The application of the GA for the determination of the model parameters, allowed for the use of the more complicated and accurate. The dark IV relationship is described in equation 1 [1].

$$I = I_{01}\left[\exp\left(\frac{q(V - IR_{SE})}{V_T}\right) - 1\right] + I_{02}\left[\exp\left(\frac{q(V - IR_{SE})}{n_2 V_T}\right) - 1\right] + \frac{(V - IR_{SE})}{R_{SH}} \quad (1)$$

where I_{01} is the saturation current of the first diode, q is the charge of an electron, R_{SE} is the lumped series resistance term, V_T is the thermal voltage and it is the product the Boltzmann constant and the absolute temperature of the cell, I_{02} is the saturation current of the second diode, n_2 is the ideality factor of the second diode and R_{SH} is the shunt resistance of the cell.

This model can also be applied to the IV data of a PV module, lumping the contributions of each current contribution of each cell into the current contributions for the whole module.

2.2. Electroluminescence

The determination of individual cell voltages can be attributed to the equation that describes the relationship of EL signal ($\emptyset_{EL}^{x,y}$) with operational voltage [2,3] (equation 2). Due to the effect of series resistance, the operational voltage ($V_O^{x,y}$) is equivalent to the applied voltage minus the potential drop due to the product of the device current and the series resistance term.

$$\emptyset_{EL}^{x,y} = C^{x,y}\, exp\left(\frac{q\, V_O^{x,y}}{V_T}\right) \quad (2)$$

where the x and y describe the pixel position, and *C* is the calibration factor.

In a study by Pothoff, et al (2010) [2], the authors determined a method to calculate the voltage distribution across the cells of a module. It is assumed that the brightest pixel ($\emptyset_{cell}^{max}$) in each cell within the images that they are well connected and must have approximately the same calibration constant. It was confirmed in the same paper, that the calibration constant for $\emptyset_{cell}^{max}$ of each cell was within ± 1.08% of the average calibration constant.

As described in the paper mentioned above, at low currents the potential drop due to the series resistance term is extremely small. At low currents the following approximation can be made:

$$V_{mod} = \sum_{i=1}^{N} V_T \ln\left(\frac{\emptyset_i^{max}}{C}\right) + I_{mod} R_{mod} \approx \sum_{i=1}^{N} V_T \ln\left(\frac{\emptyset_i^{max}}{C}\right) \quad (3)$$

where V_{mod} is the applied voltage across the module, N is the number of cells in the module, $\emptyset_i^{max}$ is the photon counts in the brightest pixel of the iᵗʰ cell, I_{mod} is the current through the module and R_{mod} is the non-cell related resistances within the circuit of the module.

Therefore, to determine the calibration constant, equation 4 is used with the data from a low current EL image.

$$C = \sqrt[N]{\frac{\prod_{i=1}^{N} \emptyset_i^{max}}{\exp\left(\frac{V_{mod}}{V_T}\right)}} \quad (4)$$

Once calibrated, it is possible to determine the individual cell voltages. Equation 5 describes the relationship between brightest pixel signal and the individual cell voltage (V_i).

$$V_i = V_T \ln\left(\frac{\emptyset_i^{max}}{C}\right) \quad (5)$$

2.3. Genetic Algorithm for Parameter Optimisation

As seen in equation 1, the I-V relation contains multiple terms, which are non-linear and implicit in nature. This hinders the formation of an explicit formula for the parameters. An optimisation procedure is used to fit the model to the data. In a study by J. Jervase [4], a Genetic Algorithm (GA) was successfully tested against simulated I-V data sets of various parameters.

Fig. 1. is the process diagram for a Genetic Algorithm. The Initialisation step is related to the generation of a population of randomised initial guesses for each parameter (individuals). The Fitness Evaluation step is a procedure in which each individual parameter set has the IV curve simulated and compared to measured data to determine their corresponding error (related to how "fit" they are). In the selection process individuals are selected for crossover where fitter individuals are favoured. Individuals' parameters are then randomly selected to be mutated within the Mutation step. Once the maximum number of iterations have been completed or the minimum threshold for error has been reached, the procedure then terminates; otherwise the process continues further.

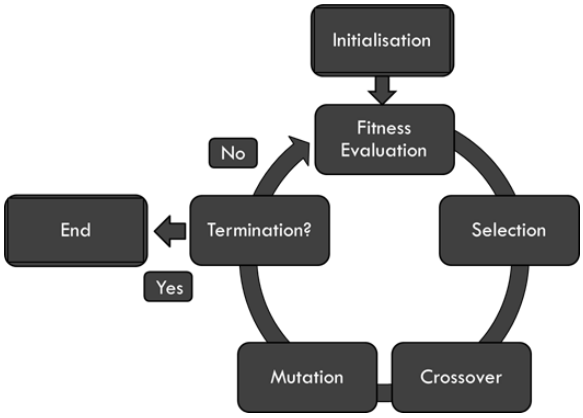

Fig. 1. Genetic Algorithm Process Diagram

3. Experimental Procedure

3.1. Device under test

The device under test was a 15.6 cm x 15.6 cm mono-crystalline Si PV module with 36 cells. The module was modified to allow for probing of individual cell voltages.

3.2 EL setup and procedure

The device was powered by a programmable DC power supply while imaged by a 1023x1024px Si CCD camera. The DC power supply was set into constant current mode allowing for the set of images to be acquired under current conditions from 0.2 A to 5.0 A in 0.2 A increments. For each resultant image taken, a dark image was acquired and subtracted from the light image to

remove stray light, thermal noise and defective pixels. Two images were obtained to remove single-time events (STEs). The procedure followed was as described in a paper by Bedrich, et al. [5]. Further noise was then removed by the application of a median filter to each image.

Even though the cells of the module are 156 mm x 156 mm ("6-inch") Si cells, the current was limited to 5 A in the experiment to accommodate the current-capacity of a damaged cell. With fully active area reduced from approximately 240 cm^2 to 91 cm^2, the remaining area had reduced electrical activity.

4. Results and discussion

4.1. EL images

The device was imaged at various operational conditions. Fig. 2. shows an EL image at 1 A and Fig. 3. is an EL image at 5 A. In both images a cracked cell (as indicated) is visible; however, in Fig. 3 the overall brightness of the cell is higher relative to the other cells. As discussed in the following section and shown in Fig. 4., this can be related to an increased relative applied voltage across the cell.

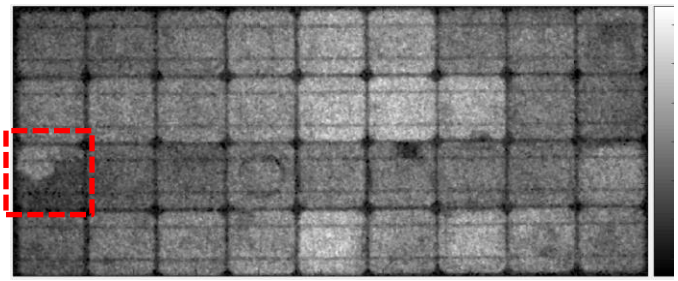

Fig. 2. EL image of the experimental module at (18.9 V, 1 A), scale from 0 counts to 100 counts)

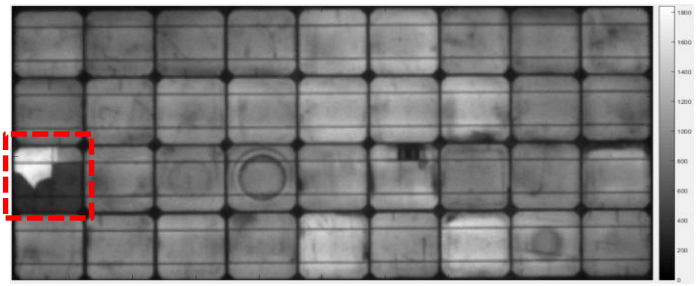

Fig. 3. EL image of the experimental module at (22 V, 5 A), scale from 0 counts to 900 counts)

4.2. Voltage distribution

Through the application of the method described in section 2.2, it was possible to determine the voltage distribution of the cells. Fig. 4. shows the deviation of each cell's voltage from the mean voltage at 1 A while Fig. 5. shows the same distribution at 5 A.

From Fig. 4. it is possible to qualitatively determine cells of lower shunt resistance relative to the other cells of the module. That is the lower voltages obtained for the cells would indicate that the shunt resistance is lower due to a lower voltage required to reach operational current. From Fig. 5., the cell indicated has a much higher potential drop across it than that of the average of the module. As observed in Fig. 2. and Fig. 3. the fully active area of this cell is reduced (from approximately 240 cm^2 to 91 cm^2) and a higher applied voltage is, therefore, required to reach the operational current.

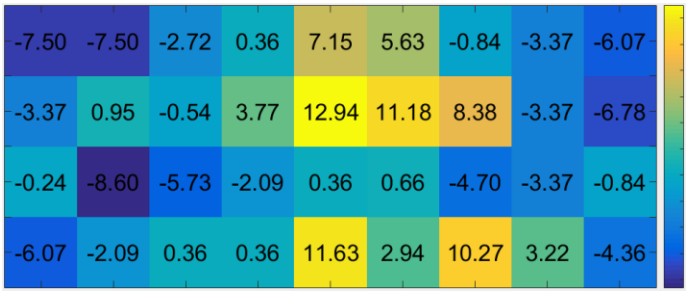

Fig. 4. Cell voltage deviation from mean (18.9 V, 1 A), scale from -8.6 mV to 12.94 mV, mean of 0.524 V

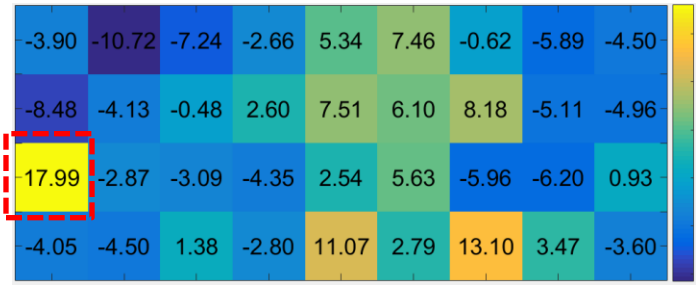

Fig. 5. Cell voltage deviation from mean (22 V, 5 A), scale from -11 mV to 18 mV, mean of 0.609 V

4.3. Cell parameter maps

The GA was successfully applied to the data to extract individual cell device parameters from voltage dependent EL images. These device parameters, corresponding to the 2-diode model are shown in Fig. 6. to Fig. 9.

Fig. 6. shows the individual cell's saturation current for the diffusion current mechanism (I_{01}). Fig. 7. shows the individual cell's saturation current for the recombination current mechanism (I_{02}). Fig. 8. shows the individual cell's ideality factor for the recombination current mechanism (n_2). Fig. 9. shows the individual cell's effective series resistance (R_{SE}). The extracted parameters identify the electrical performance of each cell. Parasitic losses can be attributed to the recombination current, series resistance and shunt current. The variability in the estimated shunt resistance values indicated that the method, as applied, could not identify shunt resistance of each cell. This is likely due to the fact that the current is low in the region of the

IV curve in which the cell does not luminesce. This limits the measurable effect of the shunt on the IV curve for this method and the ability to determine accurate cell voltages at the low currents. The variability in each cell's parameters indicates an overall mismatch within the module.

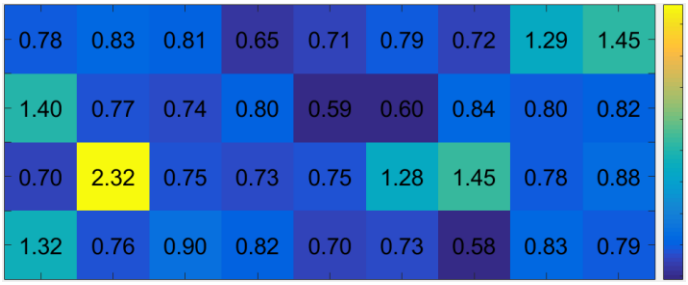

Fig. 6. Extracted I_{01} values for each cell scaled from 0.58 nA to 2.32 nA

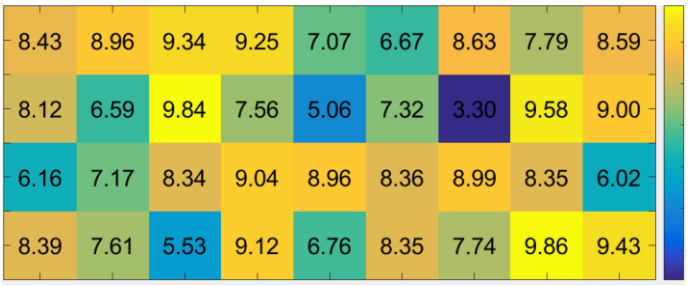

Fig. 7. Extracted I_{02} values for each cell scaled from 3.3 µA to 9.86 µA

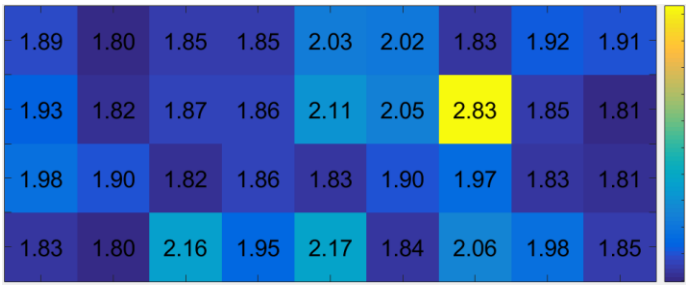

Fig. 8. Extracted n_2 values for each cell scaled from 1.8 to 2.83

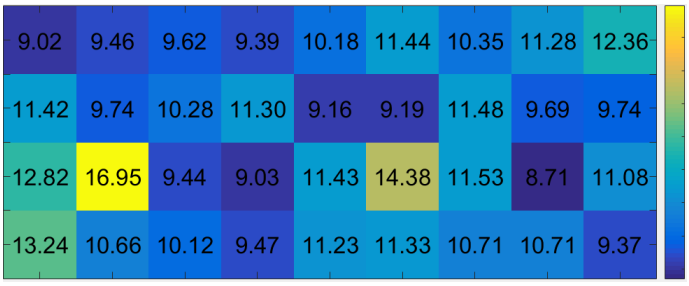

Fig. 9. Extracted R_{SE} values for each cell scaled from 8.71mΩ to 16.95mΩ

4.4. IV curve Comparison

Fig. 10. shows the comparison between the measured IV response of the module and the estimated IV response using voltage dependent EL. The estimation method has shown to be largely successful due to how well the voltages were estimated. However, the two lower voltages were less accurately determined. This is likely due to the low intensity of the EL images at low current.

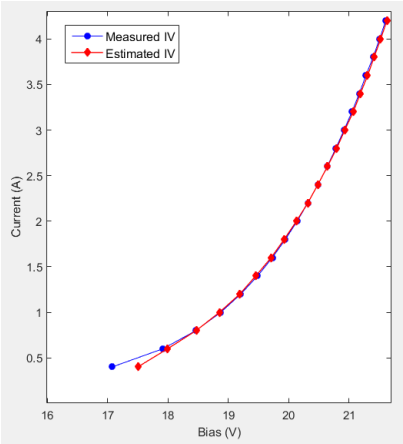

Fig. 10. Comparison between the measured IV response of the module and the estimated IV response using the voltage dependent EL

5. Conclusions

It can be concluded that voltage dependent EL image data of a PV module when combined with the dark I-V data can be used to determine the individual cell electrical characteristics. The GA was successfully utilized to extract the electrical parameters from the voltage dependent EL data and dark IV data. However, the determination of shunt resistance of each cell was shown to be relatively ineffective likely due to the fact that luminescence is limited in the voltage regions where shunt resistance effects the IV curve. Longer integration times at low voltages could yield enough voltage dependent data to determine shunt resistances. If that remains unsuccessful, voltage dependent infrared thermography can be utilised to determine the shunt resistances.

The application of this method (and future adaptations) will be used to study the effects of potential induced degradation and possibly light induced degradation of operational PV modules. This method could be used to quantify the mismatch of cells within a PV module and its degradation over the operational life of the module.

Acknowledgements

The authors would like to acknowledge the financial support from the Department of Science and Technology (DST) of South Africa, the National Research Foundation (NRF) of South Africa, PVinsight (Pty) Ltd. (PVi), the National Laser Centre (NLC) of South African through the Rental Pool Programme and Eskom.

References

[1] Pveducation.org. (2018). Double Diode Model | PVEducation. [online] Available at: http://www.pveducation.org/pvcdrom/characterisation/double-diode-model [Accessed 13 Apr. 2018].

[2] Potthoff, T., Bothe, K., Eitner, U., Hinken, D. and Köntges, M. (2010). Detection of the voltage distribution in photovoltaic modules by electroluminescence imaging. Progress in Photovoltaics: Research and Applications, 18(2), pp.100-106.

[3] Fuyuki, T. and Kitiyanan, A. (2008). Photographic diagnosis of crystalline silicon solar cells utilizing electroluminescence. Applied Physics A, 96(1), pp.189-196

[4] Jervase, J., Bourdoucen, H. and Al-Lawati, A. (2001). Solar cell parameter extraction using genetic algorithms. Measurement Science and Technology, 12(11), pp.1922-1925.

[5] K. G. Bedrich, M. Bliss, T. R. Betts, and R. Gottschalg. (2016). “ELECTROLUMINESCENCE IMAGING OF PV DEVICES : SINGLE-TIME-EFFECT STATISTICS AND REMOVAL,” in PVSAT-12, no. 1, pp. 37–40.